Article

Yanming Xu[1,†]
Dalong Li[1,†]
Ao Xue[1]
Jiaming Gu[1]
Yifan Ren[1]
Siyu Zhu[1]
Xia Lei[2]
Jianxin Liu[3]
Jihui Zhao[3]
Fang Geng[4,*]
Ning Zhang[1,*]

Calycosin-7-O-β-D-Glucoside Ameliorates Palmitate-Induced Lipid Accumulation in HT22 Cells

[1]College of Pharmacy, Heilongjiang University of Chinese Medicine, 150040 Harbin, Heilongjiang, China
[2]Jiangsu CM Clinical Innovation Center of Degenerative Bone & Joint Disease, Wuxi TCM Hospital Affiliated to Nanjing University of Chinese Medicine, 214071 Wuxi, Jiangsu, China
[3]College of Pharmacy, Hunan University of Medicine, 418000 Huaihua, Hunan, China
[4]Key Laboratory of Photochemistry Biomaterials & Energy Storage Materials of Heilongjiang Province, College of Chemistry & Chemical Engineering, Harbin Normal University, 150025 Harbin, Heilongjiang, China

Abstract

Background: The pathogenesis of Alzheimer's disease (AD) is complex. Recent research suggests that AD patients have early disorders in brain cholesterol metabolism. Cholesterol and its derivatives accumulate in neurons, leading to p-Tau overproduction and synaptic dysfunction, initiating AD progression. Calycosin-7-O-β-D-glucoside (CG), a distinctive constituent of Astragali Radix, holds a representative position. Many clinical trials have demonstrated that CG can attenuate cerebral ischemia/reperfusion injury and preserve the structural integrity of the blood-brain barrier. However, whether CG alleviates tau-mediated neurodegeneration by increasing cholesterol efflux after lipid accumulation remains unexplored.

Methods: Ultra-performance liquid chromatography/quadrupole time-of-flight mass spectrometry (UPLC-Q-TOF-MS/MS) and multivariate data analysis were employed to investigate metabolic changes in HT22 cells induced by sodium palmitate following 24 hours of CG treatment. The potential therapeutic mechanisms of CG on AD were further examined through Kyoto Encyclopedia of Genes and Genomes (KEGG) pathway enrichment analysis.

Results: Metabolomic analysis characterized 24 potential biomarkers, revealing that CG could ameliorate cholesterol metabolic pathways. The results of cell experiments revealed that CG can increase the expression of enzyme cholesterol 24-hydroxylase (CYP46A1) ($p < 0.05$) and the level of 24 hydroxycholesterol (24-OHC) ($p < 0.05$), reduce the expression of p-Tau (Thr231)/Tau ($p < 0.01$), inhibit the formation of lipid droplets.

Conclusion: CG may inhibit the accumulation of cholesterol and its derivatives in neurons by affecting the CYP46A1-CE-Tau axis, offering a potential therapeutic strategy for AD.

Keywords

cholesterol metabolism; Alzheimer's disease; calycosin-7-O-β-D-glucoside; Tau hyperphosphorylation

Introduction

Alzheimer's disease (AD) is a neurodegenerative disorder characterized by a gradual onset and progressive decline. The primary pathological features of AD include the accumulation of amyloid beta (Aβ) proteins forming senile plaques, hyperphosphorylation of Tau proteins leading to neurofibrillary tangles, and synaptic loss [1–3]. Early treatment strategies focused on Aβ, but these approaches have shown limited success in slowing disease progression,

*Corresponding author details: Fang Geng, Key Laboratory of Photochemistry Biomaterials & Energy Storage Materials of Heilongjiang Province, College of Chemistry & Chemical Engineering, Harbin Normal University, 150025 Harbin, Heilongjiang, China. E-mail: gengfang1980@163.com; Ning Zhang, College of Pharmacy, Heilongjiang University of Chinese Medicine, 150040 Harbin, Heilongjiang, China. E-mail: ningzhang1974@126.com
†These authors contributed equally.

prompting a shift towards strategies targeting Tau pathology [4]. Given that Tau pathology correlates more strongly with symptom severity than Aβ, it is a more promising target, especially once cognitive decline has begun.

The central nervous system (CNS) comprises only 2.1% of the total weight of the body but contains 23% of its sterols [5]. The brain therefore is the organ with the highest cholesterol concentration. Cholesterol is crucial for maintaining normal brain function, including cellular membrane integrity and fluidity, and it plays a pivotal role in regulating membrane transport and signal transduction. In the early stages of AD, cholesterol metabolism becomes dysregulated, accumulating cholesterol and its derivatives in neurons. This triggers excessive p-Tau production and synaptic dysfunction [6–8]. Additionally, a novel hypothesis of lipid invasion has been proposed in AD [9,10].

Most brain cholesterol is synthesized locally, with synthesis rates higher during brain development than in maturity. As the demand for cholesterol by the mature brain decreases, excess cholesterol must be efficiently removed from neurons. Excess cholesterol can be reduced to normal levels in two main ways. First, excess cholesterol is primarily converted to the hydrophilic metabolite 24-hydroxycholesterol (24-OHC) by the neuron-specific enzyme cholesterol 24-hydroxylase (CYP46A1) [11]. 24-OHC, driven by concentration gradients, diffuses across the blood-brain barrier into the systemic circulation, where its peripheral levels correlate directly with brain cholesterol levels [12]. It is subsequently transported to the liver for degradation into bile acids and excretion, which is the primary pathway for brain cholesterol elimination. Second, excess cholesterol can be excreted directly via ATP-binding cassette (ABC) transporters. CYP46A1, a hydroxylase predominantly located in hippocampal pyramidal neurons, cerebellar Purkinje cells, and the cortex, facilitates cholesterol transport and clearance in the brain. Inhibition of CYP46A1 expression leads to cholesterol overload in neurons, resulting in memory impairment and neuronal death [13]. CYP46A1 knockout (KO) mice exhibit significant learning deficits and impaired long-term potentiation (LTP). Moreover, human brain atrophy has been associated with decreased circulating levels of 24-OHC. In studies where CYP46A1 expression was knocked down in the hippocampal neurons of normal mice via adenoviruses, cognitive impairment, and increased Aβ and p-Tau production were observed [14,15].

Calycosin-7-o-β-D-glucoside (CG), a major isoflavone extracted from Astragali Radix, has been shown to reduce infarct size and protect blood-brain barrier integrity in rat models of cerebral ischemia-reperfusion (I/R) injury [16]. However, its potential to reduce neuronal lipid accumulation remains unclear. This study aimed to investigate the therapeutic effects of CG on palmitic acid (PA)-induced neuronal lipid accumulation and elucidate its underlying mechanisms.

Our findings suggest that CG activates CYP46A1 in neurons, promoting the conversion of cholesterol to 24-OHC, thereby preventing the overload of cholesterol and its associated neurotoxic effects. We hypothesize that the CYP46A1-CE-Tau axis may represent a targetable pathway in early AD, providing a theoretical basis for the development of AD therapeutics.

Materials and Methods

Reagents and Materials

The reagents and materials used in the study included HT22 cell (Mouse hippocampal neuron cell line, CX0146, Boster, Wuhan, China), CG (C823639, MACKLIN, Shanghai, China), PA (P9767, Sigma, Shanghai, China), Dulbecco's modified eagle medium (DMEM)/High glucose (SH30024.FS, Hyclone, Logan, UT, USA), Fetal Bovine Serum (FBS) (13011-0311,TIANHANG, Hangzhou, China), cell counting kit-8 (CCK-8 assay kit) (C0037, Beyotime, Shanghai, China), BeyoECL Plus (P0018S, Beyotime, Shanghai, China), rabbit anti-Tau antibody (Tau) (bs-0157R, Bioss, Shanghai, China), rabbit anti-phospho-Tau (Thr231) (p-TauThr231) antibody (bs-2368R, Bioss, Beijing, China), CYP46A1 [N1C1] antibody (GTX115492, GeneTex, SAN Antonio, TX, USA), rabbit anti-beta-actin antibody (β-actin) antibody (bs-0061R, Bioss, Beijing, China), HRP-labeled sheep anti-rabbit IgG (BM3896, Bioss, Beijing, China), total cholesterol assay kit (T-CHO assay kit) (A111-1-1, Nanjing Jiancheng Bioengineering Institute, Nanjing, China), oil red O staining kit (C0158S, Beyotime, Shanghai, China), 24-hydroxycholesterol (24-OHC) ELISA kit (JM-12385M1, JINGMEI, Shanghai, China), RIPA complete lysis buffer (P0038, Beyotime, Shanghai, China), and BCA protein assay kit (P0012S, Beyotime, Shanghai, China).

The equipment utilized included CO_2 incubator (HF90, ZHICHENG, Shanghai, China), microplate reader (MK3, Thermo Electron, Shanghai, China), Mini-PROTEAN system (Bio-Rad, Hercules, CA, USA), semi-dry electrophoretic transfer cell (Trans-Blot, Bio-Rad, Hercules, CA, USA), HPLC (AB sciex, Boston, MA, USA), and LC-Triple ToF mass spectrometer (TripleTOF 5600+, AB Sciex, Boston, MA, USA).

Grouping and Treatment

The experimental groups were organized as described. (1) Blank control: DMEM without HT22 cells. (2) Control group: HT22 cells cultured in DMEM. (3) PA groups: HT22 cells cultured in DMEM with PA at 100, 200, and 400 μM concentrations, with 6 replicate wells per group. (4) Treatment groups: HT22 cells co-cultured with CG at concentrations of 0.1, 1, 10, 100, and 1000 μM, along with the optimal CG concentration, with 6 replicate wells per group. (5) Positive control group: HT22 cells cultured in DMEM with 0.1 μM efavirenz [17].

The identity of the HT22 cell line was verified with a 98.36% match through short tandem repeat (STR) identification, ruling out cross-contamination with other cell lines. Mycoplasma testing confirmed that the HT22 cells were free from mycoplasma contamination, ensuring the reliability and accuracy of the experimental data.

Cell Viability Assay

HT22 cells were seeded in 96-well plates at a density of 1×10^3 cells per well and incubated for 24 hours. After incubation, different concentrations of the treatments were applied according to the experimental design, followed by an additional 24-hour incubation. Cell viability was assessed using the cell counting kit-8 (CCK-8) assay kit. CCK-8 reagent was added to the DMEM, and the plates were incubated at 37 °C for 2 hours. Absorbance was measured at 450 nm using a microplate reader. Cell viability was calculated using the formula: Cell viability (%) = ($A_{\text{treatment wells}}/A_{\text{control wells}}$) × 100%.

T-CHO Assay

HT22 cells were plated in 6-well plates at a density of 1×10^6 cells per well and incubated for 24 hours. Treatments were applied based on the experimental groups, followed by a 24-hour incubation. The total cholesterol (T-CHO) content in HT22 cells was measured using the T-CHO assay kit. Protein concentrations were determined with the BCA Protein Assay Kit according to the manufacturer's instructions. Cholesterol content was calculated as follows: Cholesterol content = ($A_{\text{sample}} - A_{\text{blank}}$)/($A_{\text{standard}} - A_{\text{blank}}$) × C standard/C protein. The T-CHO content results were expressed in mmol/g protein.

Metabolites and Metabolic Pathway Analysis

HT22 cells were divided into the control, model (PA, 400 μM), and CG groups (CG, 10μM). Cells (10^6–10^7) were collected using a cell scraper, centrifuged at 2500 g for 10 minutes at 4 °C, and the supernatant was discarded. The cell pellets were frozen in liquid nitrogen and subjected to three freeze-thaw cycles. Subsequently, 1 mL of 75% methanol (A: water = 3:1, v/v) was added, followed by thorough mixing, vortexing, and ultrasound disruption in an ice bath for 5 minutes. After centrifugation at 13,000 rpm for 15 minutes at 4 °C, the supernatant was collected and dried using a freeze dryer. The dried metabolites were reconstituted in methanol for injection.

Chromatographic separation was performed on the ExionL AD system (AB sciex, Boston, MA, USA) using an ACQUITY UPLC HSS T3 column (Waters, Shanghai, China) (100 mm × 2.1 mm, 1.8 μm). The column was maintained at 40 °C, and the autosampler temperature was maintained at 4 °C. The mobile phase consisted of solvent A (0.1% formic acid in water) and solvent B (0.1% formic acid in acetonitrile) (67-56-1, MACKLIN, Shanghai, China), with a gradient elution profile as follows: 0–2 min, 5% B; 2–6 min, 5%–30% B; 6–7 min, 30% B; 7–10 min, 30%–60% B; 10–11.5 min, 60% B; 11.5–13 min, 60%–80% B; 13–13.5 min, 80% B; 13.5–16 min, 80%–90% B; 16–17 min, 90% B; 17–17.5 min, 90%–100% B; 17.5–20 min, 100% B; 20–20.5 min, 100%–5% B; 20.5–23 min, 5% B. The flow rate was 0.3 mL/min, and the injection volume was 5 μL.

Mass spectrometry (MS) analysis was conducted using the SCIEX 5600+Q-TOF system (AB Sciex, Boston, MA, USA) with an electrospray ionization (ESI) source operating in the positive and negative ion modes. The ionization voltage was set at 5.5 kV (positive mode) and –4.5 kV (negative mode). The spray, auxiliary heating, and curtain gases were all set at 60 psi. The source temperature was 550 °C, with a cone voltage of 100 V and collision energies of 10 V and 40 V. The scan range for primary and secondary MS was 100–1200 m/z and 50–1200 m/z, respectively, with nitrogen used as the collision gas.

Oil Red O Staining

HT22 cells were seeded in 6-well plates at a density of 1×10^6 cells per well and incubated for 24 hours. The cells were washed twice with phosphate buffer saline, fixed with oil red O fixative for 25 minutes, and rinsed twice with water. Cells were then immersed in 60% isopropanol for 30 seconds, followed by staining with oil red O staining solu-

tion for 60 minutes. After washing with 60% isopropanol for 30 seconds and water four times, hematoxylin staining was performed for 1 minute. The stained cells were washed four times with water, treated with oil red buffer solution for 1 minute, and observed under a microscope.

Western Blot

HT22 cells were plated in 6-well plates at a density of 1×10^6 cells per well and incubated for 24 hours. The cells were then divided into Control, Model (PA, 400 μM), CG (CG, 10 μM), and Positive (Efavirenz, 0.1 μM) groups. The cell culture medium was harvested for enzyme-linked immunosorbent assay (ELISA) analysis. Cell lysates were prepared using radioimmunoprecipitation assay buffer containing protease and phosphatase inhibitors, and protein concentrations were quantified using the BCA Protein Assay kit (P0012S, Beyotime, Shanghai, China). Equal amounts of protein were loaded onto individual wells of sodium dodecyl sulfate polyacrylamide gels, and transferred to polyvinylidene fluoride (PVDF) membranes (IPVH00010, Millipore, MA, USA). Prior to further analysis, the membranes were washed with trans buffer containing 0.1% Tween 20 (TBST) (1185-53-1, Sigma, Shanghai, China) and blocked for 120 minutes in a buffer solution consisting of 5% milk. The membranes were washed three times with TBST and incubated with the primary antibodies at 4 °C overnight: Tau (1:1000, bs-0157R, Bioss, Shanghai, China), pThr231Tau (1:1000, bs-2368R, Bioss, Beijing, China), CYP46A1 [N1C1] (1:1000, GTX115492, GeneTex, SAN Antonio, TX, USA), and β-actin (1:1000, bs-0061R, Bioss, Beijing, China). The PVDF membrane was washed three times with TBST and incubated with HRP-labeled sheep anti-rabbit IgG (1:500, BM3896, Bioss, Beijing, China) for 60 minutes at room temperature. The proteins were then detected by ECL luminescence. Finally, the protein levels were quantified with ImageJ software (v1.8.0.345, NIH, Bethesda, MD, USA).

ELISA

The concentration of 24-OHC in the HT22 cell culture medium was measured using a mouse 24-OHC ELISA kit (JM-12385M1, JINGMEI, Shanghai, China). The assay was performed using a microplate reader. Blank, standard, and sample wells were prepared according to the manufacturer's instructions. A 50 μL volume of standard solution was added to the standard wells, while 40 μL of sample diluent and 10 μL of culture medium from each group were added to the sample wells. The plate was sealed and incubated at 37 °C for 30 minutes, followed by 5 washes with phosphate buffer saline (PBS). The enzyme-labeled reagent was added and incubated for another 30 minutes at 37 °C. After washing 5 times with PBS, color development was initiated with reagents A and B at 37 °C for 10 minutes. The reaction was stopped with stop solution, and the optical density (OD) was read at 450 nm. The 24-OHC concentrations were calculated based on the standard curve.

Statistical Analysis

Statistical analyses and graph generation were performed using GraphPad Prism 9 software (GraphPad Software Inc., San Diego, CA, USA). Data were presented as the averages with the standard error of the mean (SEM), derived from three independent experiments, conducted in duplicate. Differences between groups were assessed using one-way or two-way analysis of variance (ANOVA), followed by least significant difference post-hoc tests. A p-value < 0.05 was considered statistically significant.

Results

Establishment of PA-Induced Lipid Accumulation Model

Palmitic acid (PA), a saturated fatty acid, is known for inducing neuroinflammation and exacerbating neurotoxicity. *In vitro* studies have demonstrated the lipotoxic effects of PA on various cell lines, including neuronal cell lines like HT22, making it a common agent for constructing AD models [18–20]. To determine the optimal conditions for inducing lipid accumulation in HT22 cells, we exposed the cells to varying concentrations of PA for 24 hours. Total cholesterol (T-CHO) levels were measured using a T-CHO assay kit (A111-1-1, Nanjing Jiancheng Bioengineering Institute, Nanjing, China). The experimental results demonstrated that the T-CHO levels in the cells gradually increased with the increasing concentrations of PA exposure. Notably, cells treated with 400 μM PA showed a significant elevation in T-CHO levels compared to the control group ($p < 0.01$) (Fig. 1A). Consequently, a concentration of 400 μM PA was selected as the optimal condition for establishing the lipid accumulation model in HT22 cells.

Screening of Effective Protective Concentrations of CG against PA-Induced Lipid Accumulation in HT22 Cells

To identify the optimal protective concentration of calycosin-7-O-β-D-glucoside (CG) (Fig. 1B), HT22 cells were initially treated with various concentrations of CG alone for 24 and 48 hours to assess any potential cytotoxic

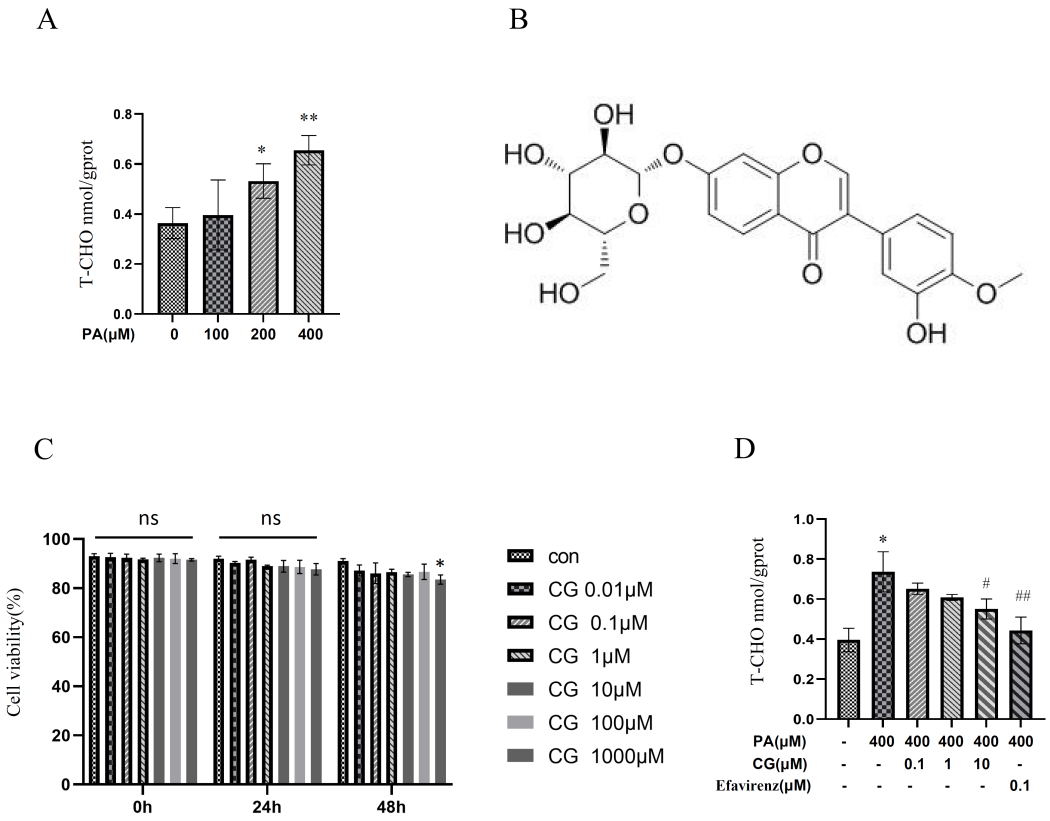

Fig. 1. The viability of HT22 cells exhibits dose-dependent responses to CG. (A) Total cholesterol (T-CHO) levels in HT22 cells after exposure to varying concentrations of PA. (B) Chemical structure of CG. (C) Viability of HT22 cells treated with different concentrations of CG for 24 or 48 hours assessed by the CCK-8 assay. (D) T-CHO content in HT22 cells following treatment with various concentrations of PA and CG. Data are presented as the mean ± standard error of the mean (SEM) from three independent experiments. Statistical significance is indicated as $^{*}p < 0.05$ and $^{**}p < 0.01$ compared to the control group; $^{\#}p < 0.05$ and $^{\#\#}p < 0.01$ compared to the PA group, not significant is indicated as ns. PA, palmitic acid; CG, calycosin-7-O-beta-D-glucoside; CCK-8, cell counting kit-8.

effects. Subsequently, the cells were co-treated with different concentrations of CG and 400 μM PA for 24 hours. The experimental results indicated that as the concentration of CG increased, the intracellular total cholesterol (T-CHO) levels gradually decreased. Notably, at a CG concentration of 10 μM, there was a significant decrease in intracellular T-CHO levels ($p < 0.05$) (Fig. 1C,D). Thus, 10 μM CG was selected as the optimal concentration for protecting HT22 cells and restoring intracellular T-CHO levels.

Multivariate Analysis of CG Effects on HT22 Cells

Raw data obtained from Ultra Performance Liquid Chromatography-Mass Spectrometry (UPLC-MS) were processed using Progenesis QI software (2.0, Waters Corporation, Milford, MA, USA) to analyze the three-dimensional information (Rt, m/z intensity) of cell samples from the control, model, and CG groups. The analysis aimed to identify the relative content and correlation of potential biomarkers in HT22 cells across the three groups. The orthogonal partial least squares discriminant analysis (OPLS-DA) plots generated by EZinfo software (3.0.3, Sartorius, Göttingen, SN, Germany) (Fig. 2A) revealed tight clustering within each group and distinct separations among the different groups. The cumulative R2Y and Q2 values for the model versus control group comparison were 0.907 and 0.592, respectively, and 0.953 and 0.596 for another comparison. A permutation test confirmed the reliability of these models, indicating that CG treatment induced sig-

Table 1. Differential metabolites identified in HT22 cells under positive and negative ion modes.

NO.	Formula	m/z	Retention time	Identification	Human metabolome database (HMDB)	Variable importance in projection (VIP)
1	$C_{42}H_{68}O_3$	620.5230	10.93	CE (5M5)	HMDB0112215	1.06739
2	$C_{45}H_{74}O_3$	662.5656	16.61	CE (dime (9, 3))	HMDB0061670	1.59791
3	$C_{48}H_{80}O_3$	727.6060	12.66	CE (monome (11, 5))	HMDB0061673	1.52999
4	$C_{49}H_{80}O_3$	739.6055	17.17	CE (11:1D5)	HMDB0112198	1.86293
5	$C_{47}H_{76}O_2$	695.5801	8.88	CE (20:4 (5Z, 8Z, 11Z, 14Z))	HMDB0006726	1.37903
6	$C_{47}H_{80}O_5$	747.5940	16.95	CE (Prostaglandin F1α)	HMDB0290249	1.13419
7	$C_{50}H_{81}NO_5S$	830.5667	20.28	CE (Leukotriene E4)	HMDB0290218	1.17199
8	$C_{43}H_{74}O_2$	623.0635	15.81	CE (16:1)	HMDB0000658	1.03300
9	$C_{27}H_{46}O_4$	457.3289	17.41	3α, 7α-dihydroxycoprostanic acid	HMDB0000359	1.56276
10	$C_{27}H_{44}O_2$	401.3414	15.81	7-ketocholesterol	HMDB0000501	2.06487
11	$C_{18}H_{33}NO$	280.2637	14.37	Linoleamide	HMDB0062656	4.36687
12	$C_{27}H_{44}O_4$	455.3129	16.17	24-hydroxycalcitriol	HMDB0006228	2.10537
13	$C_{20}H_{40}O_4$	367.2820	16.50	10, 20-dihydroxyeicosanoic acid	HMDB0031923	1.24176
14	$C_{18}H_{36}O_2$	285.2792	17.16	Stearic acid	HMDB0000827	1.08469
15	$C_{22}H_{41}NO$	336.3264	17.05	Pipericine	HMDB0031678	3.25513
16	$C_{43}H_{74}O_2$	739.6069	17.16	Oleamide	HMDB0000658	1.03152
17	$C_{18}H_{35}NO$	282.2795	15.48	LacCer (d18:1/12:0)	HMDB0002117	10.5542
18	$C_{42}H_{79}NO_{13}$	828.5506	19.53	LysoPC (18:1(9Z)/0:0)	HMDB0004866	1.63563
19	$C_{36}H_{38}O_{15}$	733.2160	19.48	Glycerol trisinapate	HMDB0036353	2.24200
20	$C_4H_6O_4$	117.0190	0.89	Succinic acid	HMDB0000254	1.26437
21	$C_9H_{11}NO_3$	180.0666	0.84	L-tyrosine	HMDB0000158	1.28322
22	$C_{11}H_{12}N_2O_2$	203.0827	2.10	L-tryptophan	HMDB0000929	2.51674
23	$C_6H_{12}O_6$	179.0544	0.63	Glucose	HMDB0000122	1.23522
24	$C_6H_{13}O_9P$	261.0371	0.59	Fructose-6-phosphate	HMDB0257695	1.23522

Note: CE, cholesterol ester.

nificant metabolic changes in HT22 cells. Volcano plots (Fig. 2B) further highlighted the metabolites that significantly contributed to the differences between the model and control groups, as well as between the CG and model groups.

Volcano plots revealed significant differences in metabolites between the model and control groups, as well as between the CG and model groups, with variable importance in projection (VIP) >1 and $p < 0.05$. A total of 24 metabolites were identified as being differentially affected by CG in HT22 cells (Table 1). To further visualize these changes, a heat map was constructed to illustrate the variations in the 24 metabolites across the control, model, and CG groups (Fig. 2C). Notably, most of the metabolite alterations observed in the model group were reversed after CG treatment, indicating that CG may help alleviate metabolic disturbances in HT22 cells.

Metabolic Pathway and Metabolite Set Enrichment Analyses

To explore the key metabolic pathways involved in the therapeutic effects of CG in AD, we conducted Kyoto Encyclopedia of Genes and Genomes (KEGG) pathway enrichment analysis using MetaboAnalyst 6.0 (https://www.metaboanalyst.ca/). The analysis revealed that the most significantly altered pathways in the metabolic pathway analysis were associated with steroid biosynthesis metabolism following CG treatment (Fig. 3A,B).

Effect of CG on CYP46A1 Protein Expression in a PA-Induced Lipid Accumulation Model in HT22 Cells

CYP46A1, a hydroxylase, promotes cholesterol transport and clearance in the brain. Efavirenz, originally marketed as an acquired immune deficiency syndrome (AIDS) drug, has been identified as a CYP46A1 agonist and is now recognized for its potential in treating AD. In this study, Efavirenz was used as a positive control drug [17]. Compared to the control group, CYP46A1 protein expres-

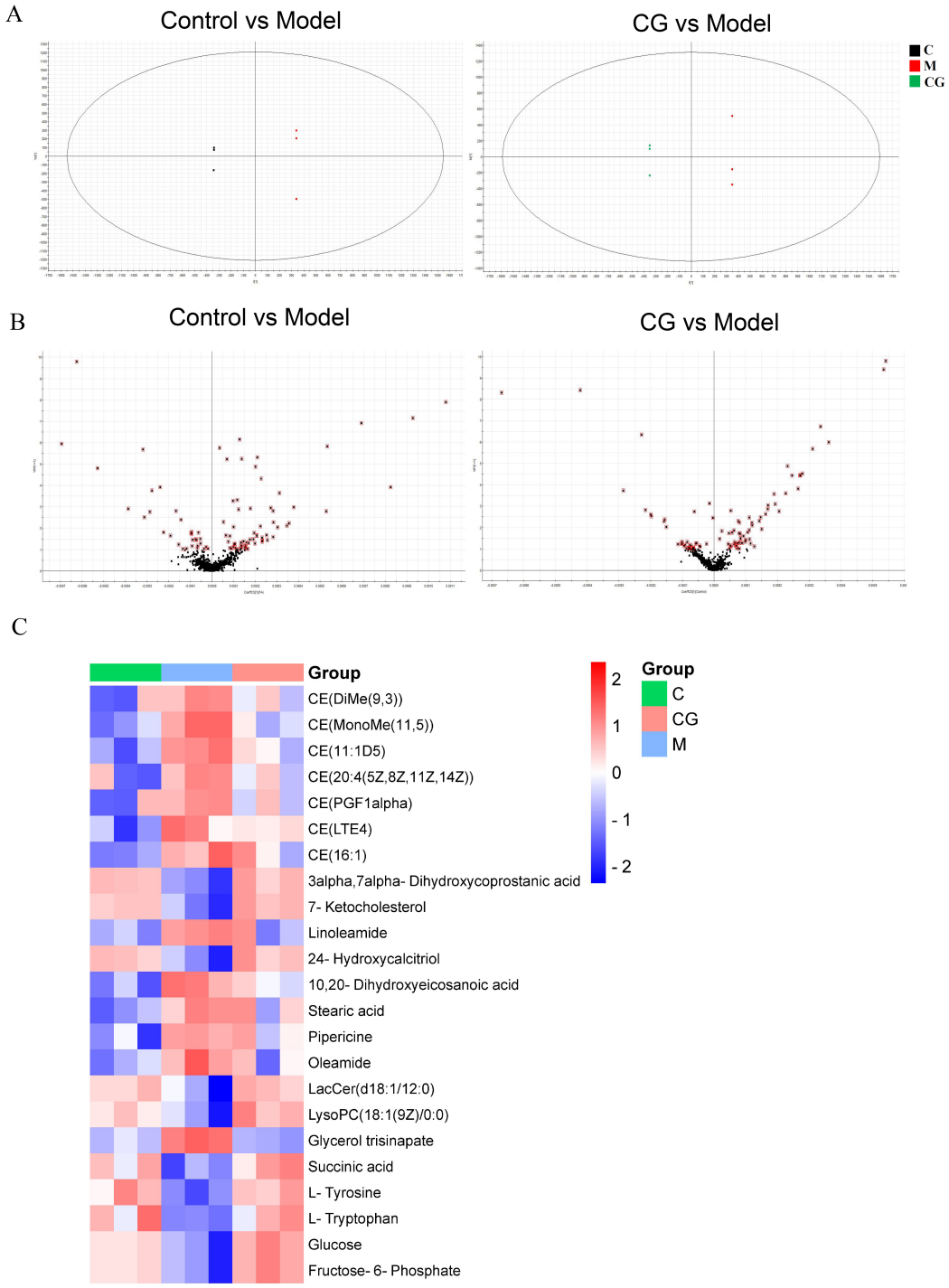

Fig. 2. Multifactorial analysis of metabolomic data in CG-treated HT22 cells. (A) OPLS-DA score plots comparing metabolites between the control, model, and CG-treated groups. (B) Volcano plot illustrating significant differences in metabolites between the model and control groups, and between the CG and model groups. (C) Heat map on the relative levels of 24 key metabolites across the control (green), model (blue), and CG (red). The color scale ranges from dark blue (lowest) to dark red (highest) metabolite levels. Abbreviations: C, control group; M, model group; CG, CG group; CG, calycosin-7-O-beta-D-glucoside; PA, palmitic acid; CE, cholesterol ester; PGF1, prostaglandin F1; LTE4, leukotriene E4.

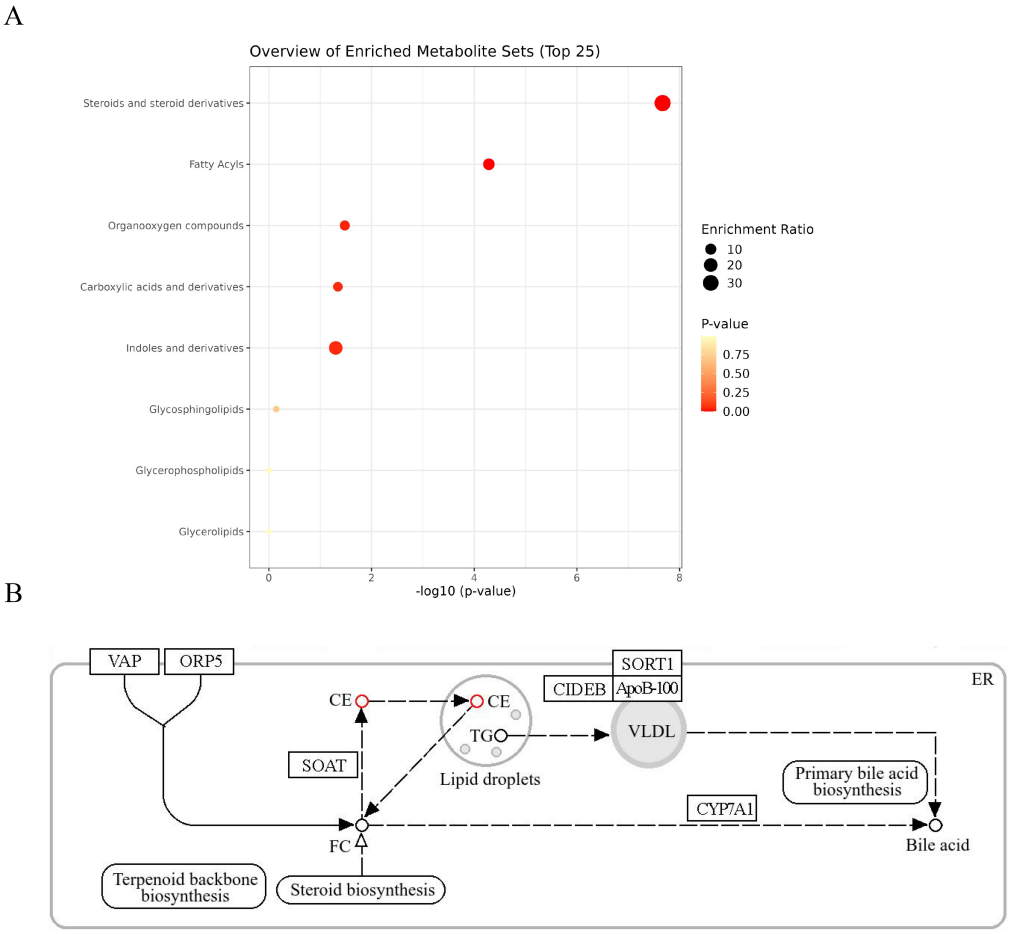

Fig. 3. Metabolite pathway analysis in CG-treated HT22 cells. (A) KEGG pathway enrichment analysis of metabolites in HT22 cells treated with CG. (B) Schematic representation of selected metabolic pathways influenced by PA and CG treatment. Abbreviations: KEGG, Kyoto Encyclopedia of Genes and Genomes; CG, calycosin-7-O-beta-D-glucoside; PA, palmitic acid; VAP, viral attachment protein; ORP5, oxysterol-binding protein-related protein 5; SOAT, sterol O-acyltransferase; FC, cholesterol; SORT1, neurotensin receptor 3; CIDEB, cell death-inducing DFFA-like effector B; VLDL, very low density lipoprotein; CYP7A1, cytochrome P450 7A1; ER, endoplasmic reticulum; TG, triacylglycerol.

sion in HT22 cells was significantly reduced in the model group ($p < 0.05$), indicating impaired cholesterol transport due to sodium palmitate. However, the positive control and CG treatment groups showed a significant increase in CYP46A1 expression compared to the model group ($p < 0.05$) (Fig. 4A,B).

Effect of CG on the Expression of Tau and p-Tau (Thr231) Protein in PA-Induced Lipid Accumulation Model in HT22 Cells

Compared to the control group, the expression of p-Tau (Thr231)/Tau in HT22 cells of the model group was significantly increased ($p < 0.05$). Compared to the model group, the expressions of p-Tau (Thr231)/Tau in HT22 cells in the positive group and CG group were significantly decreased ($p < 0.01$) (Fig. 4A–C).

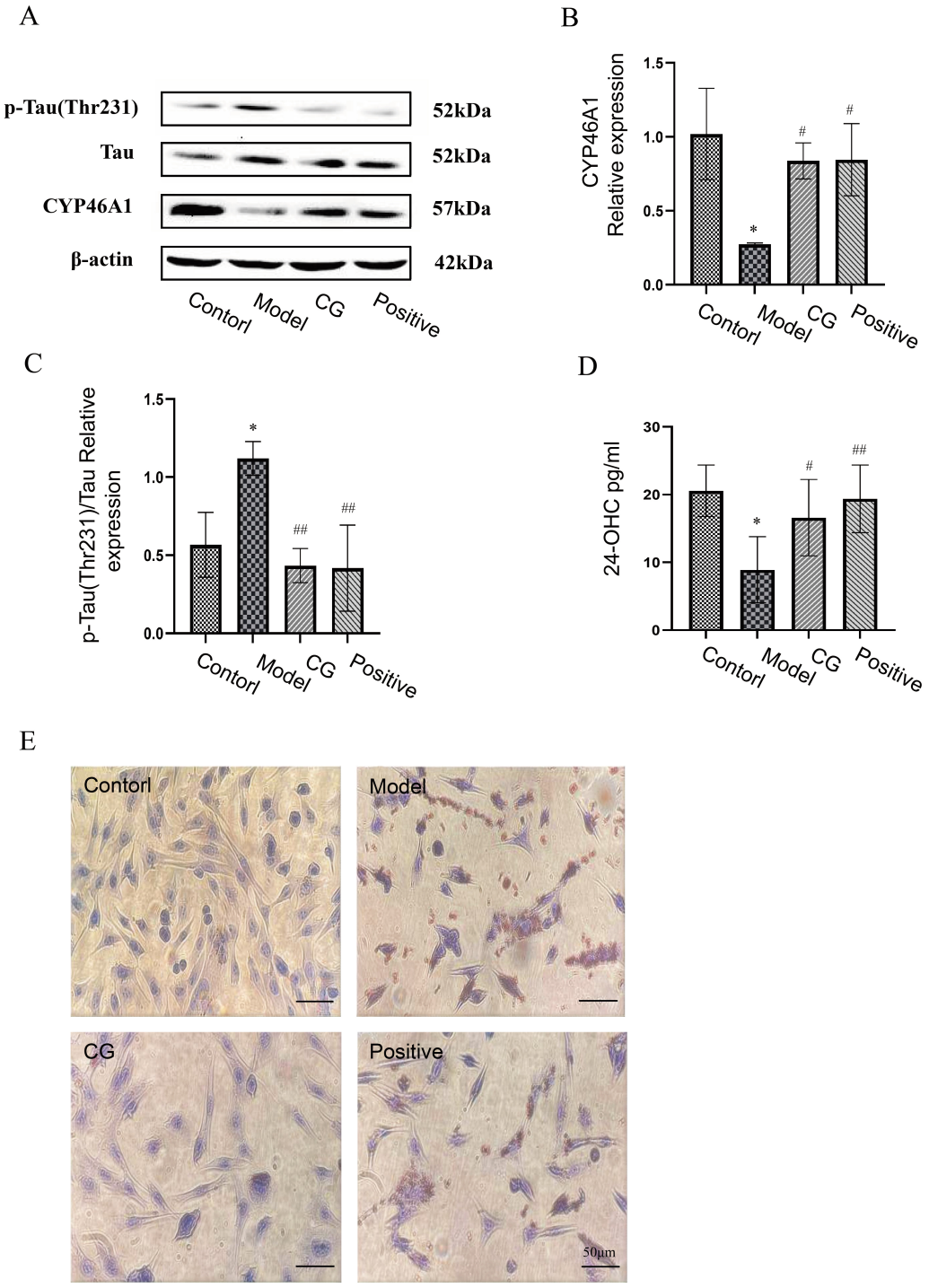

Fig. 4. Effects of CG on cholesterol metabolism in HT22 cells. (A) Western blot analysis was utilized to determine the protein expression levels of p-Tau (Thr231), Tau and CYP46A1 in HT22 cells following PA induction and CG treatment. (B,C) The signal intensity was measured quantitatively through densitometric analysis and expressed as the fold difference in comparison to the control group, both for cells treated with CG and Efavirenz. (D) ELISA was employed to assess the concentrations of 24-OHC in DMEM, following PA induction and CG treatment. (E) Staining with Oil red O. Data are presented as the mean ± SD from three independent experiments. Statistical significance is indicated as $^{*}p < 0.05$ compared to the control group; $^{\#}p < 0.05$, $^{\#\#}p < 0.01$ compared to the model group. CG, calycosin-7-O-beta-D-glucoside; PA, palmitic acid; CYP46A1, cholesterol 24-hydroxylase; DMEM, Dulbecco's modified eagle medium; SD, standard deviation; ELISA, enzyme-linked immunosorbent assay.

Effect of CG on Level of 24-OHC in PA-Induced Lipid Accumulation Model in HT22 Cells

The content of 24-OHC was significantly lower in the model group compared to the control group ($p < 0.05$). Compared to the model group, the content of 24-OHC in the CG group was increased ($p < 0.05$), and in the Positive group, it was significantly increased ($p < 0.01$) (Fig. 4D).

Effect of CG on Lipid Droplets in a PA-Induced Lipid Accumulation Model in HT22 Cells

Compared to the control group, the number of HT22 cells stained with oil red in the model group was increased significantly, and the formation of lipid droplets was obvious in the cells. Compared to the model group, there were significantly fewer HT22 cells stained with oil red in the positive group and the CG group, and there was no obvious visible lipid droplet formation in the cells (Fig. 4E).

Discussion

Cholesterol is esterified in the endoplasmic reticulum and stored in cytoplasmic lipid droplets as cholesterol ester (CE). When needed, CE can be hydrolyzed back to cholesterol by acid lipase in the lysosome. In the brain, CE accounts for approximately 1% of total cholesterol [21]. Accumulation of CE and lipid droplets has been observed in the AD brain [22]. Disruptions in cholesterol homeostasis, such as those caused by apolipoprotein E deficiency or cholesterol overload, can lead to a 1.8-fold increase in CE levels, positively correlated with AD progression. Recent study [8] has shown that CE can independently regulate the production of Tau and β-amyloid proteins through distinct pathways. A key pathological feature of AD is the hyperphosphorylation of Tau protein, leading to its detachment from microtubules, abnormal folding, aggregation, and formation of neurofibrillary tangles (NFTs), which contribute to neuronal injury and synaptic dysfunction [23].

Calycosin-7-O-β-D-glucoside (CG), the principal component of Astragali Radix (AR), a traditional Chinese medicine, is known for its protective effects against cerebral ischemia-reperfusion injury and for maintaining blood-brain barrier integrity [7]. However, its potential neuroprotective effects in neurodegenerative diseases have remained unclear. The current study demonstrates that CG inhibits PA-induced lipid accumulation in neurons, suggesting its therapeutic potential in AD.

Consistent with these findings, our metabolomics analysis revealed significant increases in CE and triglyceride (TG) levels in the PA-induced HT22 lipid accumulation model, identifying CE and TG as the primary components of lipid droplets. Notably, all eight detected CE species were significantly elevated in this model (Fig. 2, Table 1). Although free cholesterol levels remained unchanged, CG significantly reduced total cholesterol (free + esterified cholesterol) by decreasing CE levels (Fig. 1).

24-Hydroxycholesterol (24-OHC) is recognized for its neuroprotective properties, partly by enhancing α-secretase activity to regulate amyloid precursor protein (APP) processing [24]. Research has found that injecting adeno-associated virus-cholesterol 24-hydroxylase (AAV-CYP46A1) into the hippocampus of AD mice reduces Aβ plaque formation and restores spatial memory [25]. Similarly, upregulation of CYP46A1 expression in 5XFAD mice improves cognitive behavior. Moreover, 24-OHC, an endogenous activator of liver X receptors (LXR), upregulates ATP-binding cassette transporter A1 (ABCA1) and ATP binding cassette transporter G1 (ABCG1) expression, promoting cholesterol efflux [26]. The levels of CYP46A1 and 24-OHC in the hippocampus of THY-Tau22 mice were significantly lower compared to control mice. Restoration of CYP46A1 levels in the hippocampus led to improvements in memory, dendritic length, and spine density, and normalization of long-term potentiation (LTP) [27]. In AD mouse models, restoring neuronal CYP46A1 level improves cholesterol metabolism, inhibits APP processing, prevents synaptic loss, and improves cognitive dysfunction [28]. Consistent with these findings, our study observed that CG upregulated CYP46A1 expression and increased 24-OHC secretion.

At the same time, the number of lipid droplets was observed by oil red O staining. Compared to the control group, the density of small lipid droplet like structures increased significantly in model group, indicating an increase in lipid and cholesterol storage in the PA-induced HT22 lipid accumulation model. The metabolomics results indicate that CG can significantly reduce the levels of TG and CE in the PA-induced HT22 lipid accumulation model and inhibit lipid droplet formation, which was closely related to its effect on p-Tau (Thr231)/Tau in these neurons (Fig. 4). These findings suggest that CG mitigates Tau hyperphosphorylation by promoting 24-OHC-mediated cholesterol efflux in the HT22 lipid accumulation model, thereby offering a potential therapeutic mechanism for AD.

Conclusion

In conclusion, the neuroprotective effects of CG may be attributed to the activation of CYP46A1 within neurons, which promotes the conversion and excretion of cholesterol into 24-OHC, thereby inhibiting abnormal cholesterol accumulation and reducing PA-induced damage to HT22 cells.

Availability of Data and Materials

Data will be made available on request from corresponding authors.

Author Contributions

YMX and DLL designed the research study. AX, JMG, YFR and SYZ performed the research. NZ acquired the data. XL, JXL and JHZ analyzed the data. FG interpreted the data. NZ and FG drafted this manuscript. All authors contributed to important editorial changes in the manuscript. All authors read and approved the final manuscript. All authors have participated sufficiently in the work and agreed to be accountable for all aspects of the work.

Ethics Approval and Consent to Participate

Not applicable.

Acknowledgment

Not applicable.

Funding

This work was supported by Heilongjiang Provincial Administration of Traditional Chinese Medicine (ZHY2023-051), National Natural Science Foundation of China, China (General Program, 82174007).

Conflict of Interest

The authors declare no conflict of interest.

References

[1] Olloquequi J, Ettcheto M, Cano A, Sanchez-López E, Carrasco M, Espinosa T, *et al*. Impact of New Drugs for Therapeutic Intervention in Alzheimer's Disease. Frontiers in Bioscience (Landmark Edition). 2022; 27: 146.

[2] Busche MA, Hyman BT. Synergy between amyloid-β and tau in Alzheimer's disease. Nature Neuroscience. 2020; 23: 1183–1193.

[3] Lane CA, Hardy J, Schott JM. Alzheimer's disease. European Journal of Neurology. 2018; 25: 59–70.

[4] Golde TE. Disease-Modifying Therapies for Alzheimer's Disease: More Questions than Answers. Neurotherapeutics: the Journal of the American Society for Experimental NeuroTherapeutics. 2022; 19: 209–227.

[5] Dai L, Zou L, Meng L, Qiang G, Yan M, Zhang Z. Cholesterol Metabolism in Neurodegenerative Diseases: Molecular Mechanisms and Therapeutic Targets. Molecular Neurobiology. 2021; 58: 2183–2201.

[6] Luo J, Yang H, Song BL. Mechanisms and regulation of cholesterol homeostasis. Nature Reviews. Molecular Cell Biology. 2020; 21: 225–245.

[7] Loera-Valencia R, Goikolea J, Parrado-Fernandez C, Merino-Serrais P, Maioli S. Alterations in cholesterol metabolism as a risk factor for developing Alzheimer's disease: Potential novel targets for treatment. The Journal of Steroid Biochemistry and Molecular Biology. 2019; 190: 104–114.

[8] van der Kant R, Langness VF, Herrera CM, Williams DA, Fong LK, Leestemaker Y, *et al*. Cholesterol Metabolism Is a Druggable Axis that Independently Regulates Tau and Amyloid-β in iPSC-Derived Alzheimer's Disease Neurons. Cell Stem Cell. 2019; 24: 363–375.e9.

[9] Rudge JD. A New Hypothesis for Alzheimer's Disease: The Lipid Invasion Model. Journal of Alzheimer's Disease Reports. 2022; 6: 129–161.

[10] Varma VR, Büşra Lüleci H, Oommen AM, Varma S, Blackshear CT, Griswold ME, *et al*. Abnormal brain cholesterol homeostasis in Alzheimer's disease-a targeted metabolomic and transcriptomic study. NPJ Aging and Mechanisms of Disease. 2021; 7: 11.

[11] Petrov AM, Pikuleva IA. Cholesterol 24-Hydroxylation by CYP46A1: Benefits of Modulation for Brain Diseases. Neurotherapeutics: the Journal of the American Society for Experimental NeuroTherapeutics. 2019; 16: 635–648.

[12] Li D, Zhang J, Liu Q. Brain cell type-specific cholesterol metabolism and implications for learning and memory. Trends in Neurosciences. 2022; 45: 401–414.

[13] Sodero AO. 24S-hydroxycholesterol: Cellular effects and variations in brain diseases. Journal of Neurochemistry. 2021; 157: 899–918.

[14] Popiolek M, Izumi Y, Hopper AT, Dai J, Miller S, Shu HJ, *et al*. Effects of CYP46A1 Inhibition on Long-Term-Depression in Hippocampal Slices *ex vivo* and 24S-Hydroxycholesterol Levels in Mice *in vivo*. Frontiers in Molecular Neuroscience. 2020; 13: 568641.

[15] Mitroi DN, Pereyra-Gómez G, Soto-Huelin B, Senovilla F, Kobayashi T, Esteban JA, *et al*. NPC1 enables cholesterol mobilization during long-term potentiation that can be restored in Niemann-Pick disease type C by CYP46A1 activation. EMBO Reports. 2019; 20: e48143.

[16] Li M, Han B, Zhao H, Xu C, Xu D, Sieniawska E, *et al*. Biological active ingredients of Astragali Radix and its mechanisms in treating cardiovascular and cerebrovascular diseases. Phytomedicine: Inter-

national Journal of Phytotherapy and Phytopharmacology. 2022; 98: 153918.

[17] Mast N, El-Darzi N, Petrov AM, Li Y, Pikuleva IA. CYP46A1-dependent and independent effects of efavirenz treatment. Brain Communications. 2020; 2: fcaa180.

[18] Beaulieu J, Costa G, Renaud J, Moitié A, Glémet H, Sergi D, *et al*. The Neuroinflammatory and Neurotoxic Potential of Palmitic Acid Is Mitigated by Oleic Acid in Microglial Cells and Microglial-Neuronal Co-cultures. Molecular Neurobiology. 2021; 58: 3000–3014.

[19] Lu P, Yan HJ, Yang C, Feng WC, Hu F, Wu YY, *et al*. High fat suppresses SOD1 activity by reducing copper chaperone for SOD1 associated with neurodegeneration and memory decline. Life Sciences. 2021; 272: 119243.

[20] Phitthayaphong P, Kumfu S, Chattipakorn N, Chattipakorn SC. Blockage of Fc Gamma Receptors Alleviates Neuronal and Microglial Toxicity Induced by Palmitic Acid. Journal of Alzheimer's Disease: JAD. 2021; 82: 1315–1332.

[21] Hansen SB. Cholesterol's Function and Origin in the Alzheimer's Disease Brain. Journal of Alzheimer's Disease: JAD. 2023; 94: 471–472.

[22] Hu ZL, Yuan YQ, Tong Z, Liao MQ, Yuan SL, Jian Y, *et al*. Re-examining the Causes and Effects of Cholesterol Deposition in the Brains of Patients with Alzheimer's Disease. Molecular Neurobiology. 2023; 60: 6852–6868.

[23] Saher G. Cholesterol Metabolism in Aging and Age-Related Disorders. Annual Review of Neuroscience. 2023; 46: 59–78.

[24] Gamba P, Giannelli S, Staurenghi E, Testa G, Sottero B, Biasi F, *et al*. The Controversial Role of 24-S-Hydroxycholesterol in Alzheimer's Disease. Antioxidants (Basel, Switzerland). 2021; 10: 740.

[25] Alavi MS, Karimi G, Ghanimi HA, Roohbakhsh A. The potential of CYP46A1 as a novel therapeutic target for neurological disorders: An updated review of mechanisms. European Journal of Pharmacology. 2023; 949: 175726.

[26] Petrov AM, Lam M, Mast N, Moon J, Li Y, Maxfield E, *et al*. CYP46A1 Activation by Efavirenz Leads to Behavioral Improvement without Significant Changes in Amyloid Plaque Load in the Brain of 5XFAD Mice. Neurotherapeutics: the Journal of the American Society for Experimental NeuroTherapeutics. 2019; 16: 710–724.

[27] Wu M, Zhang M, Yin X, Chen K, Hu Z, Zhou Q, *et al*. The role of pathological tau in synaptic dysfunction in Alzheimer's diseases. Translational Neurodegeneration. 2021; 10: 45.

[28] Wang T, Cui S, Hao L, Liu W, Wang L, Ju M, *et al*. Regulation of Th17/Treg Balance by 27-Hydroxycholesterol and 24S-Hydroxycholesterol Correlates with Learning and Memory Ability in Mice. International Journal of Molecular Sciences. 2022; 23: 4370.